



CHEMISTRY & SUSTAINABILITY

CHEM **SUS** CHEM

ENERGY & MATERIALS

Accepted Article

Title: Mesoporogen-Free Synthesis of Nano-sized Hierarchical SAPO-34 Zeolite with Reduced Template Consumption and Excellent MTO Performance

Authors: Qiming Sun, Ning Wang, Risheng Bai, Guangrui Chen, Zhiqiang Shi, Yongcun Zou, and Jihong Yu

This manuscript has been accepted after peer review and appears as an Accepted Article online prior to editing, proofing, and formal publication of the final Version of Record (VoR). This work is currently citable by using the Digital Object Identifier (DOI) given below. The VoR will be published online in Early View as soon as possible and may be different to this Accepted Article as a result of editing. Readers should obtain the VoR from the journal website shown below when it is published to ensure accuracy of information. The authors are responsible for the content of this Accepted Article.

To be cited as: *ChemSusChem* 10.1002/cssc.201801486

Link to VoR: <http://dx.doi.org/10.1002/cssc.201801486>

WILEY-VCH

www.chemsuschem.org

A Journal of



Mesoporogen-Free Synthesis of Nano-sized Hierarchical SAPO-34 Zeolite with Reduced Template Consumption and Excellent MTO Performance

Qiming Sun,^[a] Ning Wang,^[a] Risheng Bai,^[a] Guangrui Chen,^[a] Zhiqiang Shi,^[a] Yongcun Zou,^[a] and Jihong Yu^{*[a, b]}

Abstract: A great interest has emerged in the development of nano-sized and hierarchical SAPO-34 zeolites because of their enhanced accessibility and improved catalytic activity in methanol-to-olefin (MTO) conversions. Here a series of nano-sized SAPO-34 catalysts with tunable hierarchical structures are synthesized in the system of $\text{Al}_2\text{O}_3\text{-H}_3\text{PO}_4\text{-SiO}_2\text{-triethylamine(TEA)-H}_2\text{O}$ by using a mesoporogen-free nanoseed-assistant method. The nano-sized hierarchical $\text{S}_{\text{H}}\text{-3.0}$ catalyst ($\text{TEA}/\text{Al}_2\text{O}_3=3.0$) possesses the highest crystallinity, abundant intracrystalline meso/macropores, and suitable acidity among all of the obtained catalysts, showing the highest selectivity of ethylene and propylene up to 85.4%. This value reaches the top level in MTO reactions ever reported under the similar conditions. Detailed coke analyses reveal that the small-sized methyl-substituted benzene and bulky methyl-substituted pyrene are mainly located inside the crystals instead of on the surface of crystals, which provides further insight into the understanding of the deactivation of the SAPO-34 catalyst during MTO reaction. Significantly, the simple and cost-effective synthetic process and superb catalytic performance of the nano-sized hierarchical SAPO-34 promise their practical large-scale application in future MTO units.

Introduction

Microporous crystalline zeolites with ordered pore architectures and uniform channels and/or cavities have been widely used as the most important solid heterogeneous catalysts in various industrial processes due to the excellent shape selectivity and superior thermal and hydrothermal stability.^[1] Silicoaluminophosphate zeolite SAPO-34 with **CHA** topological structure has drawn tremendous attention due to the superior selectivity of light olefins in methanol-to-olefin (MTO) conversion, which has proven to be one of the most successful non-petrochemical routes for the production of light olefins.^[2] SAPO-34 zeolite possesses small three-dimensional 8-ring pore openings and a large *cha* cage as well as moderate acidity, which

can induce a very high selectivity of light olefins in MTO reactions with complete conversion of methanol.^[3] However, the severe diffusion limitation and rapid coke formation often lead to the rapid deactivation and unsatisfactory light olefins selectivity during methanol conversion, which greatly decreases the economic benefit of commercial MTO process.^[4] Hence, retarding coke deposition rate, prolonging the catalytic lifetime as well as enhancing the light olefins selectivity of SAPO-34 catalysts in MTO reaction are highly desired.

Decreasing the crystal size to nanoscale can effectively reduce the formation rate of coke deposition and improve the catalytic activity during MTO conversions. Tetraethylammonium hydroxide (TEAOH) is the most commonly-used template to synthesize nano-sized SAPO-34 crystals, but the high prices force researchers to find other cheaper alternatives.^[5] Triethylamine (TEA), as a cheap and commercially available organic compound, is also a frequently-used template to generate SAPO-34 catalysts.^[3e, 6] However, the large micron-sized crystal and intergrowth phase of SAPO-34 (**CHA**)/SAPO-18 (**AEI**) usually give rise to the suboptimal MTO catalytic performance, especially the lower selectivity of ethylene and propylene. So it is highly desired to synthesize nano-sized SAPO-34 catalysts in the absence of SAPO-18 impurity using cheap templates.

Besides the reduction of crystal sizes, fabrication of hierarchically porous structure can also significantly improve the intercrystalline mass transport efficiency for the reactant and products as well as enhance the catalytic activity in MTO reactions.^[7] Various methods, such as hard-templating method,^[7f, 7g] soft-templating method,^[7d, 7e, 8] and post-treatment method^[9] have been employed to generate the hierarchical SAPO-34 catalysts. While, these above approaches not only usually need to add extra mesoporogen or additionally tedious operation, but also result in phase separation, poor crystallinity as well as low stability. Recently, our group developed a novel seed-assisted method to synthesize nano-sized hierarchical SAPO-34 catalysts using excess TEA as the template, which exhibited an excellent selectivity of ethylene plus propylene (85%).^[10] The superfluous consumption of organic templates undoubtedly brings the increase of synthetic cost and environmental pollution. So it still needs to further optimize synthetic conditions and reduce the consumption of organic templates on the premise of keeping the excellent MTO catalytic performance.

In this work, a series of nano-sized hierarchical SAPO-34 catalysts with tunably hierarchical structures and physicochemical properties were synthesized using different amounts of TEA as the template by mean of the *in-*

[a] Dr. Q. Sun, Dr. N. Wang, R. Bai, G. Chen, Z. Shi, Dr. Y. Zou, Prof. J. Yu
State Key Laboratory of Inorganic Synthesis and Preparative Chemistry, College of Chemistry, Jilin University
2699 Qianjin Street, Changchun, 130012, People's Republic of China
E-mail: jihong@jlu.edu.cn

[b] Prof. J. Yu
International Center of Future Science, Jilin University
2699 Qianjin Street, Changchun, 130012, People's Republic of China

Supporting information for this article is given via a link at the end of the document.

situ mesopore-free nanoseed-assistant method. The zeolitic phase and crystallinity, the sizes and distributions of meso/macropores and the acidity of samples are significantly subjected to the additions of TEA in the synthetic gel. Owing to the assistance of seeds, the pure SAPO-34 catalyst without SAPO-18 and SAPO-5 impurity can be obtained with a TEA/Al₂O₃ ratio of 2.0. Significantly, the nano-sized hierarchical SAPO-34 catalyst synthesized with a TEA/Al₂O₃ ratio of 3.0 possesses high crystallinity, abundant intracrystalline meso/macropores and suitable acidity, showing the longest catalytic lifetime and highest selectivity of ethylene plus propylene up to 85.4%, which is the top level in the MTO reaction ever reported under similar conditions. As compared with our previous work, the consumption of organic template was reduced 40 percent.^[10] In addition, according to the detailed coke analyses, we find that the small-sized methyl-substituted benzene and bulky methyl-substituted pyrene are prone to be generated inside the channels of crystals instead of on the outer surface of crystals. Compared to the conventional microporous catalyst, the hierarchical catalysts are capable to accommodate more amounts of larger coke species avoiding rapid deactivation.

Results and Discussion

The hierarchical SAPO samples (S_{H-x}) are synthesized by adding different amounts of TEA as the template together with some nano-sized seeds. The synthetic gels with molar compositions of 1.0Al₂O₃: 1.0P₂O₅: xTEA: 0.4SiO₂: 70H₂O: 8.0 wt% Seeds (x = 5.0 ~ 0.2) are crystallized under hydrothermal conditions at 200 °C for 36 h. The nano-sized seeds are prepared using the TEOH as the template. The SAPO-34 seeds have the pure CHA topological structure and nanosheet-like morphology with the size of about 200 nm (Figure S1 in the Supporting Information). The microporous SAPO samples (S_{M-x}) are synthesized with the similar gel compositions of hierarchical S_{H-x} samples except for the absence of seeds.

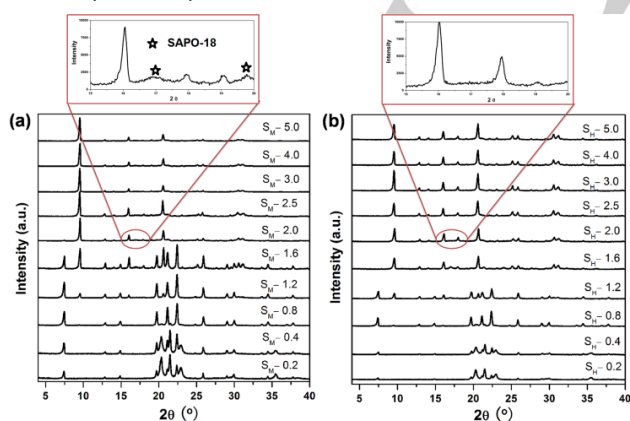


Figure 1. XRD patterns of a) micron-sized microporous SAPO zeolites (S_{M-x}) and b) nano-sized hierarchical SAPO zeolites (S_{H-x}).

The XRD patterns of microporous S_{M-x} and hierarchical S_{H-x} samples are shown in Figure 1. Without adding seeds, the SAPO-34 with some impurity of SAPO-18 can be obtained when the TEA/Al₂O₃ ratio is more than 2.0. The content of SAPO-18 gradually increases with the decrease of TEA amount. When the TEA/Al₂O₃ ratio is less than 2.0, the diffraction peaks of SAPO-5 can be detected. When further decreasing the TEA/Al₂O₃ ratio less than 1.2, the pure SAPO-5 zeolite is obtained. In contrast, introducing the seeds into the synthetic gel is beneficial for the formation of SAPO-34 zeolite. With the assistance of seeds, the pure SAPO-34 zeolite can be produced with the TEA/Al₂O₃ ratio more than 2.0. The mixed phase of SAPO-34 and SAPO-18 can be formed with the TEA/Al₂O₃ ratio of 1.6. When the ratio of TEA/Al₂O₃ further decreases to less than 1.6, the SAPO-5 zeolites start to appear.

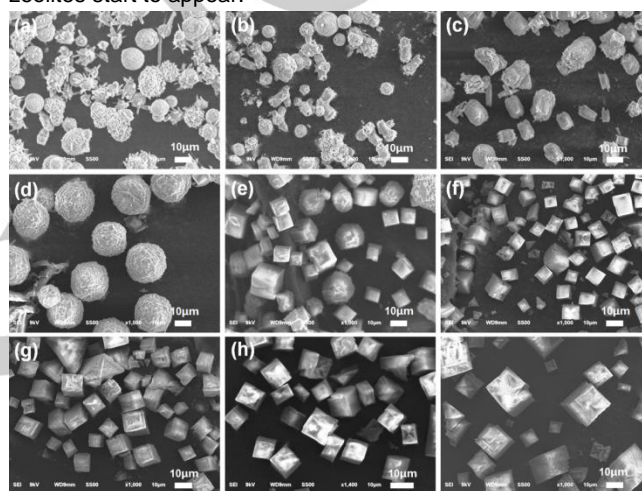


Figure 2. SEM images of micron-sized microporous SAPO zeolites (S_{M-x}). a) S_{M-0.2}, b) S_{M-0.4}, c) S_{M-0.8}, d) S_{M-1.2}, e) S_{M-1.6}, f) S_{M-2.0}, g) S_{M-3.0}, h) S_{M-4.0}, and i) S_{M-5.0}. The scale bars of all images are 10 μm.

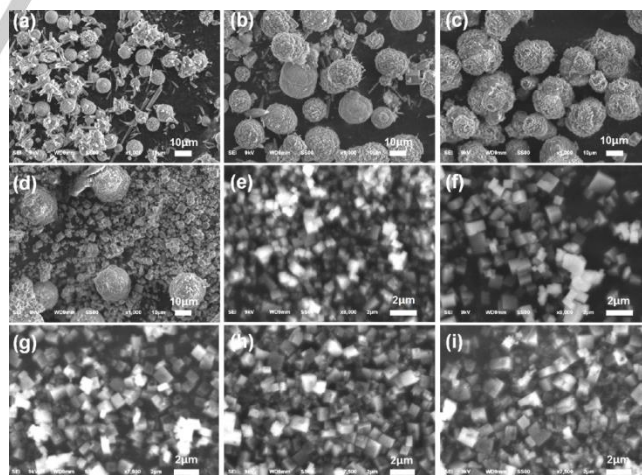


Figure 3. SEM images of nano-sized hierarchical SAPO zeolites (S_{H-x}). a) S_{H-0.2}, b) S_{H-0.4}, c) S_{H-0.8}, d) S_{H-1.2}, e) S_{H-1.6}, f) S_{H-2.0}, g) S_{H-3.0}, h) S_{H-4.0}, and i) S_{H-5.0}. The scale bars of images a-d) are 10 μm, and the scale bars of images e-i) are 2 μm.

SEM images of microporous SAPO zeolites S_{M-x} and hierarchical S_{H-x} samples are shown in Figures 2 and 3. The

micron-sized floriated SAPO-5 crystals can be observed in both of S_{M-x} ($x = 0.2 \sim 1.6$) and S_{H-x} ($x = 0.2 \sim 1.2$) samples. However, for the SAPO-34 crystals, the S_{H-x} ($x = 1.6 \sim 5.0$) samples exhibit remarkably reduced crystal sizes (200–800 nm) as compared with S_{M-x} ($x = 2.0 \sim 5.0$) samples ($\sim 10 \mu\text{m}$). TEM images clearly reveal the presence of mesopores and macropores with sizes of 20 ~ 150 nm extending along the nanocrystals of samples $S_{H-4.0}$, $S_{H-3.0}$, $S_{H-2.0}$, and $S_{H-1.6}$. Moreover, with the increase of TEA addition, more hierarchical pores can be formed, and the pore sizes are gradually enlarged (Figure 4).

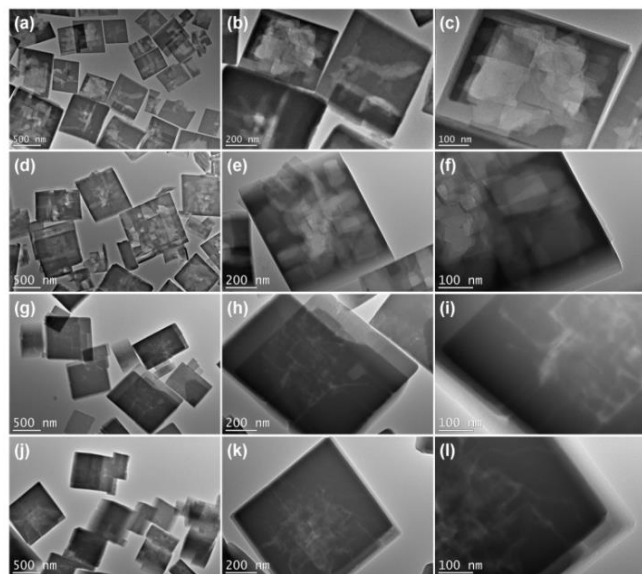


Figure 4. TEM images of nano-sized hierarchical samples (S_{H-x}). a-c) $S_{H-4.0}$, d-f) $S_{H-3.0}$, g-i) $S_{H-2.0}$, j-l) $S_{H-1.6}$. Scale bars: a, d, g, j) 500 nm, b, e, h, k) 200 nm, and c, f, i, l) 100 nm.

The microporous sample $S_{M-4.0}$ and hierarchical samples $S_{H-4.0}$, $S_{H-3.0}$, $S_{H-2.0}$, and $S_{H-1.6}$ display the characteristics of type-I N_2 adsorption-desorption isotherms (Figure 5a). Compared with sample $S_{M-4.0}$, an apparent

uptake near saturation pressure in the isotherms of all hierarchical SAPO-34 samples can be observed, which can be attributed to the presence of voids between the nano-sized crystals stacking and the existence of mesopores and/or macropores in the hierarchical SAPO-34 crystals.^[3h, 11] This is in accordance with the observation of SEM and TEM images. Moreover, the nano-sized hierarchical samples $S_{H-4.0}$, $S_{H-3.0}$, $S_{H-2.0}$, and $S_{H-1.6}$ exhibit the increased microporous areas (553–519 m^2/g), micropore volumes (0.26–0.25 cm^3/g) and mesopore volumes (0.09–0.10 cm^3/g) as compared with the micron-sized microporous SAPO-34 sample $S_{M-4.0}$ (511 m^2/g , 0.24 cm^3/g , and 0.03 cm^3/g). Notably, the hierarchical sample $S_{H-3.0}$ shows the highest microporous area (553 m^2/g), indicating the highest crystallinity among all of the samples. The detailed N_2 adsorption-desorption results are summarized in Table 1. Meanwhile, the pore size distributions also reveal the existence of hierarchical porosity in samples $S_{H-4.0}$, $S_{H-3.0}$, $S_{H-2.0}$, and $S_{H-1.6}$ (Figure 5b).

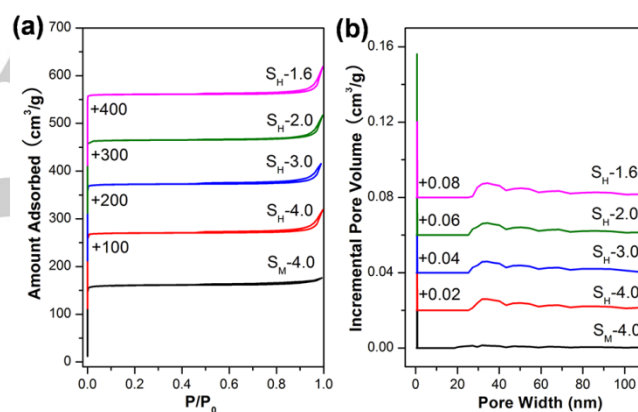


Figure 5. a) N_2 adsorption-desorption, b) Density functional theory pore size distribution curves of micron-sized microporous ($S_{M-4.0}$) and nano-sized hierarchical SAPO-34 ($S_{H-4.0}$, $S_{H-3.0}$, $S_{H-2.0}$, and $S_{H-1.6}$) samples.

Table 1. Framework composition and porosity of micron-sized microporous SAPO-34 ($S_{M-4.0}$) and nano-sized hierarchical SAPO-34 ($S_{H-4.0}$, $S_{H-3.0}$, $S_{H-2.0}$, and $S_{H-1.6}$) samples.

Samples	Molar Composition ^[a]	S_{BET} ^[b] [m^2/g]	S_{micro} ^[c] [m^2/g]	S_{ext} ^[c] [m^2/g]	V_{micro} ^[c] [cm^3/g]	V_{meso} ^[d] [cm^3/g]
$S_{M-4.0}$	$\text{Al}_{0.48}\text{P}_{0.40}\text{Si}_{0.12}\text{O}_2$	528	511	17	0.24	0.03
$S_{H-4.0}$	$\text{Al}_{0.49}\text{P}_{0.40}\text{Si}_{0.11}\text{O}_2$	558	547	11	0.26	0.09
$S_{H-3.0}$	$\text{Al}_{0.49}\text{P}_{0.41}\text{Si}_{0.10}\text{O}_2$	566	553	13	0.26	0.10
$S_{H-2.0}$	$\text{Al}_{0.49}\text{P}_{0.42}\text{Si}_{0.09}\text{O}_2$	541	528	13	0.25	0.09
$S_{H-1.6}$	$\text{Al}_{0.48}\text{P}_{0.43}\text{Si}_{0.09}\text{O}_2$	528	519	9	0.25	0.10

[a] Measured by inductively coupled plasma (ICP) spectrometer; [b] S_{BET} (total surface area) is calculated by applying the BET equation using the linear part ($0.05 < P/P_0 < 0.30$) of the adsorption isotherm; [c] S_{micro} (micropore area), S_{ext} (external area), and V_{micro} (micropore volume) are calculated using the t-plot method; [d] V_{meso} (mesoporous volume) is calculated using the BJH method (from desorption)

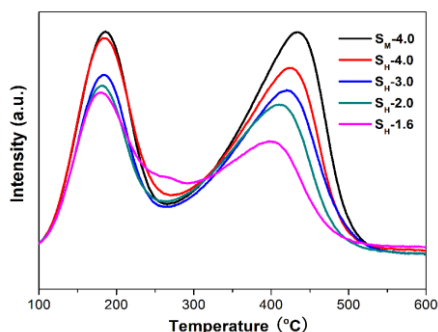


Figure 6. NH_3 -TPD curves of micron-sized microporous SAPO-34 (S_M -4.0) and nano-sized hierarchical SAPO-34 (S_H -4.0, S_H -3.0, S_H -2.0 and S_H -1.6) samples.

Thermogravimetry (TG) analyses show that the SAPO-34 samples exhibit more weight loss as compared with the SAPO-5 samples, indicating that more organic templates are located inside the channels of SAPO-34 (Figures S2 and S3 in the Supporting Information). With the decrease of organic templates added in the synthetic gel, the SAPO-34 samples show fewer weight losses. Meanwhile, the silicon contents of samples are gradually reduced along with the decrease of added templates in the synthetic gels, and the introduction of seed can further decrease the silicon contents of samples (Table 1 and S1 in the Supporting Information). ^{29}Si MAS NMR results reveal that all of the obtained samples possess the similar local silicon atomic environments (Figure S4 in the Supporting Information). The $\text{Si}(\text{O}(\text{Si}4\text{Al}))$ unit with the peak at ca. -90 ppm as the main silicon species exists in all of the samples.^[12] Compared with the conventional microporous sample, the hierarchical samples possess more $\text{Si}(\text{OAl})_n(\text{OH})_{4-n}$ unit with the shoulder peak ranging from -80 to -90 ppm attributed to the breaking of the $\text{Si}-\text{OH}-\text{Al}$ bond, indicating the existence of defects or/and hierarchical structures. Note that the difference of Si contents of samples can considerably affect the acidity of SAPO-34 samples. As shown in Figure 6, with the decrease of silicon contents, the acidities of SAPO-34 samples are correspondingly reduced.

The MTO catalytic performances of micron-sized microporous SAPO-34 (S_M -4.0) and nano-sized hierarchical SAPO-34 (S_H -4.0, S_H -3.0, S_H -2.0, and S_H -1.6) samples are evaluated at 450 °C with a WHSV of 4 h^{-1} in a fix-bed reactor. The catalytic lifetime and selectivity of ethylene and propylene of samples are shown in Figure 7. The detailed catalytic results and product distribution of samples are given in Figures S5-S9 in the Supporting Information and Table 2. Compared to the micron-sized microporous catalyst S_M -4.0, the nano-sized hierarchical catalysts (S_H -4.0, S_H -3.0, and S_H -2.0) with pure SAPO-34 phase exhibit more than a twice prolonged catalytic lifetime and considerably improved the selectivity of ethylene and propylene. Notably, the nano-sized hierarchical catalyst S_H -3.0 shows the longest catalytic lifetime of 366 min and the highest selectivity of ethylene plus propylene up to 85.4%, which are much higher than those of the microporous

catalyst S_M -4.0 (126 min, 79.7%) and other hierarchical catalysts S_H -4.0 (326 min, 84.9%), S_H -2.0 (326 min, 82.4%), and S_H -1.6 (306 min, 78.1%). The MTO catalytic performance of catalyst S_H -3.0 is the top level in MTO reactions ever reported under the similar conditions.^[3h, 8a] More importantly, under the same catalytic condition (450 °C, WHSV = 4 h^{-1}) compared with our previous work, the S_H -3.0 catalyst possess more than 40% decreased consumption of organic template and 0.7% enhanced selectivity of ethylene and propylene (the detailed catalytic results of our previous work are shown in Table 2 and Figure S10 in the Supporting Information).^[10]

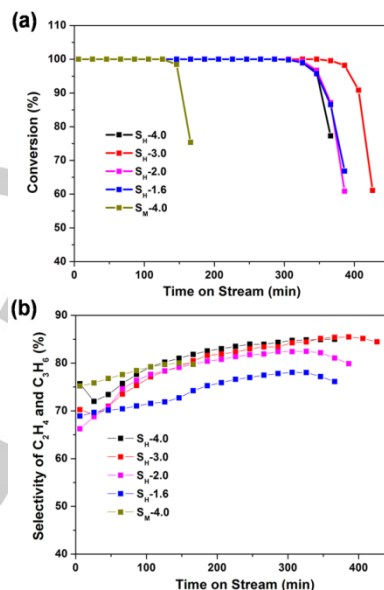


Figure 7. a) Lifetimes and b) selectivity of ethylene and propylene over micron-sized microporous SAPO-34 (S_M -4.0) and nano-sized hierarchical SAPO-34 (S_H -4.0, S_H -3.0, S_H -2.0 and S_H -1.6) samples. Experimental conditions: WHSV = 4 h^{-1} , T = 450 °C, catalyst weight = 300 mg.

Compared with the conventional microporous S_M -4.0, the enhanced catalytic property of hierarchical catalysts can be attributed to the decreased crystal size, high crystallinity of pure **CHA** phase, abundant hierarchical structure, and decreased acidity. Among all of the hierarchical SAPO-34 catalysts, the S_H -3.0 exhibits the longest lifetime and highest selectivity of ethylene and propylene, which can be mainly attributed to its highest crystallinity, and the suitable acidity and hierarchical structure. Considering the similar hierarchical structure and crystallinity with S_H -4.0, the improved catalytic performance of S_H -3.0 is mainly attributed to the decreased acidity, which can restrain the coke formation rate. In comparison with S_H -2.0, the enhanced catalytic activity of S_H -3.0 is mainly ascribed to the higher crystallinity and larger mesoporous sizes that is beneficial for the transport of methanol and products. Note that although possessing the lowest acidity, nano-sized and hierarchical structure, the S_H -1.6 catalyst with mixed phases of SAPO-34 and SAPO-18 exhibits remarkably decreased selectivity of ethylene, and the final selectivity of ethylene and propylene is only 78.1%. This result demonstrates that

the SAPO-34 catalyst is beneficial for the formation of light olefins than the SAPO-18 catalyst, and effectively avoiding the formation of SAPO-18 impurity in the SAPO-34 catalyst is of great significance to improve the catalytic performance in MTO conversion.

After MTO reactions, the coke species retained on the surface and inside the deactivated catalysts are examined by gas chromatography-mass spectrometer (GC-MS) analyses. To analyze the coke species on the surface of the SAPO-34 catalyst, the deactivated SAPO-34 catalyst was carefully ground for 5 min, and then the solid was extracted by CH_2Cl_2 . To get the total coke species, the deactivated catalyst was etched by HF solution for 24 h and then extracted by CH_2Cl_2 . The total coke species in the samples are shown in Figure 8a. More bulky cokes such as multi-methyl-substituted pyrene can be detected within the deactivated hierarchical SAPO-34 catalysts as compared with the microporous SAPO-34 catalyst. Interestingly, the coke species on the surface of both hierarchical and microporous catalysts are much the same. Multi-methyl-substituted naphthalene, multi-methyl-substituted anthracene, and pyrene as the main coke species are located on the surface of catalysts, but few methyl-substituted benzenes and bulky multi-methyl-substituted pyrene species can be detected on the surface of catalysts (Figure 8b). Figure 8c shows a schematic of coke distribution in the deactivated SAPO-34 catalyst. Above results might shed some light to understand the reason of deactivation for the SAPO-34 catalyst during the MTO reaction. In previous work, the methyl-substituted benzene species are considered as the active intermediates for the generation of ethylene and propylene.^[13] According to the coke analyses, the reason for the deactivation of conventional microporous SAPO-34 catalysts is mainly caused by the blocks on the outer surface, instead of the absence of active intermediates. Severe coke depositions on the outer surface of SAPO-34 catalysts lead to inaccessibility of methanol and active sites or/and active intermediates inside the catalyst, even though the active intermediates still exist within the deactivated catalysts; this is consistent with previous works.^[14] Moreover, our experimental results clearly reveal that the bulky multi-methyl-substituted pyrene is located inside the intracrystalline hierarchical spaces, which demonstrates that fabricating hierarchical structure is a powerful approach to benefit for the interaction between methanol and active intermediates, accommodating more bulky coke species,

and avoiding fast deactivation. When the meso/macropores in hierarchical SAPO-34 catalysts are filled with cokes, the deactivation is inevitable due to the inaccessibility of the methanol into the active sites. However, compared with the microporous counterparts, the hierarchical SAPO-34 catalysts can maximize the use of active sites and possess the prolonged lifetime and enhanced activity in MTO reactions.

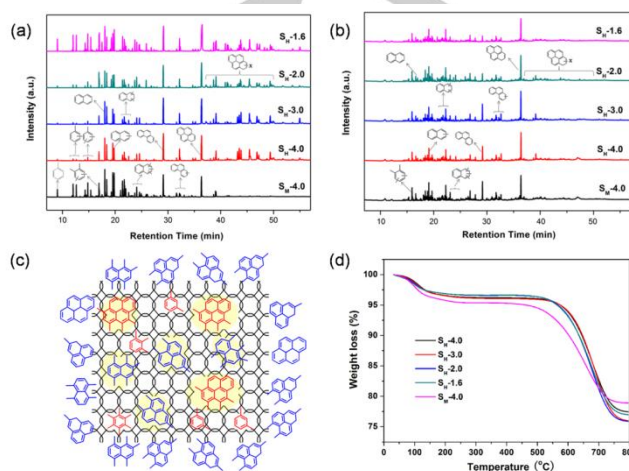


Figure 8. GC-MS chromatograms of a) total coke species and b) coke species on the surface in deactivated micron-sized microporous ($S_M-4.0$) and nano-sized hierarchical SAPO-34 ($S_H-4.0$, $S_H-3.0$, $S_H-2.0$, and $S_H-1.6$) samples after methanol conversions at 450 °C. c) A schematic of coke deposition in the deactivated SAPO-34 catalyst. d) TG curves of deactivated micron-sized microporous ($S_M-4.0$) and nano-sized hierarchical SAPO-34 ($S_H-4.0$, $S_H-3.0$, $S_H-2.0$, and $S_H-1.6$) samples after methanol conversions at 450 °C.

TG analyses of deactivated catalysts reveal that the weight loss (20.04 ~ 21.62%) and the decomposition temperature of cokes (550 ~ 750 °C) in the hierarchical catalysts are higher than that in the conventional microporous catalyst (18.08% and 450 ~ 700 °C), which further confirms that more amounts of bulky polycyclic aromatic hydrocarbon are located inside the hierarchical catalysts (Figure 8d and Table S2). Significantly, the hierarchical catalysts $S_H-3.0$ shows the lowest coke deposition rate of 0.14 mg min^{-1} among the catalysts, which is more than twice decrease than that of conventional microporous SAPO-34 catalyst (0.32 mg min^{-1}) (Table S2 in the Supporting Information).

Table 2. MTO results on micron-sized microporous ($S_M-4.0$), nano-sized hierarchical SAPO-34 ($S_H-4.0$, $S_H-3.0$, $S_H-2.0$, and $S_H-1.6$), and counterpart catalysts.

Catalysts	Lifetime ^[a] [min]	Selectivity[%]							
		CH ₄	C ₂ H ₄	C ₂ H ₆	C ₃ H ₆	C ₃ H ₈	C ₄	C ₅ ⁺	C ₂ ⁺ +C ₃ ⁺
$S_M-4.0$	126	1.7	43.3	0.8	36.4	3.0	10.7	4.1	79.7
$S_H-4.0$	326	2.2	50.0	0.5	34.9	0.7	8.4	3.3	84.9
$S_H-3.0$	366	2.6	51.3	0.6	34.1	0.7	7.8	2.9	85.4
$S_H-2.0$	326	3.4	47.6	0.5	34.8	0.5	9.2	4.0	82.4
$S_H-1.6$	306	4.0	43.1	0.5	35.0	0.9	11.2	5.3	78.1
Counterpart ^[b]	286	2.3	50.1	0.5	34.6	0.7	8.4	3.4	84.7

Reaction conditions: WHSV = 4 h⁻¹, T = 450 °C, catalyst weight = 300 mg.

[a] Lifetime: the reaction duration with > 99.9% methanol conversion. [b] The counterpart catalyst was a nano-sized hierarchical SAPO-34 catalyst reported in our previous work,^[10] which was synthesized with the ratio of TEA/Al₂O₃ = 4.7.

Conclusions

In summary, a facile and cost-effective mesopore-free method has been developed for the synthesis of nano-sized SAPO-34 catalysts with tunable hierarchical structures and physicochemical properties by using TEA as the sole template. The pure SAPO-34 catalyst without SAPO-18 and SAPO-5 impurity can be obtained with a TEA/Al₂O₃ ratio as low as 2.0. Significantly, the nano-sized hierarchical SAPO-34 catalyst with the lower TEA/Al₂O₃ ratio of 3.0 shows the excellent selectivity of ethylene and propylene up to 85.4% due to high crystallinity, abundant intracrystalline meso/macropores, and suitable acidity. Such value is among the highest level in the MTO reaction ever reported under the similar conditions. Detailed coke analyses reveal that the small-sized methyl-substituted benzene species and bulky methyl-substituted pyrene are prone to be generated inside spaces instead of on the surface of catalysts. The above results reveal that the main reason for the catalyst deactivation is the blockage of the outer surface of the SAPO-34 catalyst instead of the lack of active intermediates. Therefore, fabricating hierarchical structure has proven to be a powerful method to promote the contact between methanol and active intermediates as well as avoid fast deactivation. More importantly, the facile and cost-effective synthetic process and outstanding catalytic performance of nano-sized hierarchical SAPO-34 zeolite catalysts promise their practical large-scale application in MTO units.

Experimental Section

Chemicals and Materials. Aluminum iso-propoxide (Al(OPr)₃, 99.5 wt%, Beijing Reagents Company), pseudoboehmite (Al₂O₃, 62.5 wt%, Vista), phosphoric acid (H₃PO₄, 85 wt%, Beijing Chemical Works), tetraethylammonium hydroxide solution (TEAOH, 35 wt%, Alfa Aesar), triethylamine (TEA, 99%, Fuyu Company), colloidal silica (40 wt%, Aldrich), fumed silica (Changling Refining Company), hydrofluoric acid (HF, 40 wt%, Beijing Chemical Works), dichloromethane (CH₂Cl₂, Biaoshiqi Reagents Company).

Synthesis of nanosheet-like SAPO-34 zeolite seeds. The nanosheet-like SAPO-34 zeolite seeds were synthesized under conventional hydrothermal conditions from a starting gel with the molar composition of Al₂O₃/P₂O₅/TEAOH/SiO₂/H₂O = 1.0/1.2/2.0/0.6/40 as reported in our previous work.^[5a]

Synthesis of nano-sized hierarchical SAPO-34 zeolites. The nano-sized hierarchical SAPO-34 zeolites were synthesized with the molar compositions of 1.0Al₂O₃: 1.0P₂O₅: xTEA: 0.4SiO₂: 70H₂O: 8.0 wt% Seeds (x = 5.0, 4.0, 3.0, 2.5, 2.0, 1.6, 1.2, 0.8, 0.4, and 0.2) under hydrothermal conditions at 200 °C for 36 h, and the resulting products were named as S_H-x (x meant the molar ratio of TEA/Al₂O₃). Typically, the pseudoboehmite was added into the mixture of deionized water and phosphoric acid solution, followed by a continuous stirring for 2 h. Then the TEA was added to the above mixture. After a continuous stirring for 1 h, the fumed silica was added into the resultant solution and then stirred for 2 h

continuously. Finally, 8.0 wt% of SAPO-34 seed was added into the mixture and then stirred continuously until the seed was dissolved completely. The synthetic gel was transferred to a stainless steel autoclave and heated at 200 °C for 36 h. The as-synthesized solid product was calcined in air at 550 °C for 8 h to remove the template.

Synthesis of micron-sized microporous SAPO-34 zeolites. The micron-sized microporous SAPO-34 zeolites were synthesized with the molar compositions of 1.0Al₂O₃: 1.0P₂O₅: xTEA: 0.4SiO₂: 70H₂O (x = 5.0, 4.0, 3.0, 2.5, 2.0, 1.6, 1.2, 0.8, 0.4, and 0.2) under hydrothermal conditions at 200 °C for 36 h, and the resulting products were named as S_M-x (x meant the molar ratio of TEA/Al₂O₃). The synthetic procedure is similar to that of nano-sized hierarchical SAPO-34 zeolites except for the absence of seeds.

Characterizations. Powder X-ray diffraction patterns recorded on a Rigaku D-Max 2550 diffractometer using Cu K α radiation (λ = 0.15418 nm) were used to identify the zeolite phases. The morphologies of catalysts were measured by transmission electron microscopy (TEM) (Tecnai F20 electron microscope) and scanning electron microscopy (SEM) (JSM-6510 (JEOL) electron microscope). Thermogravimetric (TG) analysis was performed on a TGA Q500 unit in the air with a heating rate of 10 °C min⁻¹ from room temperature to 800 °C in air. Chemical compositions of samples were analyzed by inductively coupled plasma (ICP) using Perkin-Elmer Optima 3300 DV ICP instrument. The acidity of samples was measured by ammonia temperature-programmed desorption of ammonia (NH₃-TPD) experiments (Micromeritics AutoChem II 2920 automated chemisorption analysis unit). N₂ adsorption/desorption measurements were carried out on a Micromeritics 2020 analyzer at 77.35 K after the samples were degassed at 350 °C under vacuum. ²⁹Si NMR spectra were performed on a Bruker AVANCE III 400 WB spectrometer.

Catalytic Tests and Carbon Deposit Analyses. MTO reaction was performed in a fixed-bed reactor at atmospheric pressure. 300 mg of catalysts (40-60 mesh) were loaded in the quartz reactor (6 mm inner diameter) and activated at 500 °C in an N₂ flow (30 mL min⁻¹) for 1 h before starting each reaction. Then the temperature was adjusted to reaction temperature (450 °C), and the methanol was fed by passing the carrier gas (N₂, 15 mL/min) through a saturator containing methanol at 49 °C, which gave a WHSV of 4.0 h⁻¹. The products were analyzed using an online gas chromatograph (Agilent GC 7890N), equipped with a flame ionization detector (FID) and Plot-Q column (Agilent J&W GC Columns, HP-PLOT/Q 19091P-Q04, 30 m x 320 μ m x 20 μ m). The conversion and selectivity were calculated on the CH₂ basis and dimethyl ether was considered as a reactant in the calculation.

The coke deposition amounts of deactivated SAPO-34 catalysts (the final methanol conversion decreased to about 60%) after the MTO reactions were determined by TG analyses. To analyze the coke species on the surface of the SAPO-34 catalyst, the deactivated SAPO-34 catalysts were carefully ground for 5 min, and then the solid was extracted by CH₂Cl₂, the obtained solutions were analyzed by GC-MS (Thermo Fisher Trace ISQ, equipped with TG-5MS column, 60 m x 320 μ m x 25 μ m). To determine the total coke species, the deactivated catalysts were etched by HF solution for 24 h, and then extracted by CH₂Cl₂. Subsequently, the obtained solutions were analyzed by GC-MS.

Acknowledgements

This work was supported by the Nation Key Research and Development Program of China (Grant No. 2016YFB0701100), National Natural Science Foundation of China (Grant Nos. 21320102001, and 21621001) and the National 111 Project (B17020).

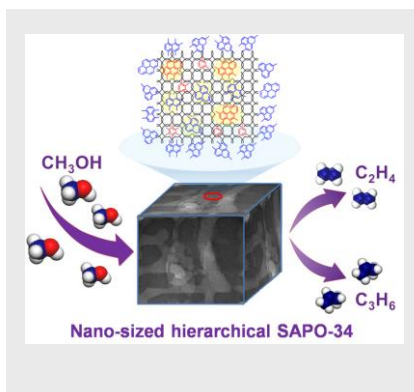
Keywords: heterogeneous catalysis • methanol-to-olefin • zeolites • SAPO-34 • low template consumption

- [1] a) A. Corma, *Chem. Rev.* **1997**, *97*, 2373-2420; b) W. J. Roth, P. Nachtigall, R. E. Morris, J. Čejka, *Chem. Rev.* **2014**, *114*, 4807-4837; c) J. Čejka, A. Corma, S. I. Zones, Zeolites and catalysis: synthesis reactions and applications, Wiley-VCH, Weinheim, **2010**, pp. 1-881; d) W. Schwieger, A. G. Machoke, T. Weissenberger, A. Inayat, T. Selvam, M. Klumpp, A. Inayat, *Chem. Soc. Rev.* **2016**, *45*, 3353-3376; e) M.-H. Sun, S.-Z. Huang, L.-H. Chen, Y. Li, X.-Y. Yang, Z.-Y. Yuan, B.-L. Su, *Chem. Soc. Rev.* **2016**, *45*, 3479-3563; f) D. Verboekend, N. Nuttens, R. Locus, J. Van Aelst, P. Verolme, J. C. Groen, J. Perez-Ramirez, B. F. Sels, *Chem. Soc. Rev.* **2016**, *45*, 3331-3352; g) Y. Li, L. Li, J. Yu, *Chem* **2017**, *3*, 928-949; h) Q. Sun, N. Wang, Q. Bing, R. Si, J. Liu, R. Bai, P. Zhang, M. Jia, J. Yu, *Chem* **2017**, *3*, 477-493; i) S. Lopez-Orozco, A. Inayat, A. Schwab, T. Selvam, W. Schwieger, *Adv. Mater.* **2011**, *23*, 2602-2615; j) L.-H. Chen, X.-Y. Li, J. C. Rooke, Y.-H. Zhang, X.-Y. Yang, Y. Tang, F.-S. Xiao, B.-L. Su, *J. Mater. Chem.* **2012**, *22*, 17381-17403; k) K. Na, M. Choi, R. Ryoo, *Microporous Mesoporous Mater.* **2013**, *166*, 3-19.
- [2] a) C. D. Chang, *Catal. Rev.* **1984**, *26*, 323-345; b) P. Tian, Y. X. Wei, M. Ye, Z. M. Liu, *ACS Catal.* **2015**, *5*, 1922-1938; c) J. Zhong, J. Han, Y. Wei, P. Tian, X. Guo, C. Song, Z. Liu, *Catal. Sci. Technol.* **2017**, *7*, 4905-4923; d) Q. Sun, Z. Xie, J. Yu, *Natl. Sci. Rev.* **2018**, *5*, 542-558; e) U. Olsbye, S. Svelle, M. Bjørgen, P. Beato, T. V. W. Janssens, F. Joensen, S. Bordiga, K. P. Lillerud, *Angew. Chem. Int. Ed.* **2012**, *51*, 5810-5831; *Angew. Chem.* **2012**, *124*, 5910-5933. f) D. Chen, K. Moljord, A. Holmen, *Microporous Mesoporous Mater.* **2012**, *164*, 239-250.
- [3] a) W. Dai, X. Wang, G. Wu, N. Guan, M. Hunger, L. Li, *ACS Catal.* **2011**, *1*, 292-299; b) M. Li, Y. Wang, L. Bai, N. Chang, G. Nan, D. Hu, Y. Zhang, W. Wei, *Appl. Catal. A* **2017**, *531*, 203-211; c) Y. Gao, S.-L. Chen, Y. Wei, Y. Wang, W. Sun, Y. Cao, P. Zeng, *Chem. Eng. J.* **2017**, *326*, 528-539; d) D. Zhao, Y. Zhang, Z. Li, Y. Wang, J. Yu, *Chem. Eng. J.* **2017**, *323*, 295-303; e) J. Zhu, Y. Li, U. Muhammad, D. Wang, Y. Wang, *Chem. Eng. J.* **2017**, *316*, 187-195; f) Q. Sun, N. Wang, G. Guo, J. Yu, *Chem. Commun.* **2015**, *51*, 16397-16400; g) H. Yang, Z. Liu, H. Gao, Z. Xie, *J. Mater. Chem.* **2010**, *20*, 3227-3231; h) Q. Sun, N. Wang, G. Guo, X. Chen, J. Yu, *J. Mater. Chem. A* **2015**, *3*, 19783-19789; i) Y. Jin, Q. Sun, G. Qi, C. Yang, J. Xu, F. Chen, X. Meng, F. Deng, F.-S. Xiao, *Angew. Chem., Int. Ed.* **2013**, *52*, 9172-9175; *Angew. Chem.* **2013**, *125*, 9342-9345 j) G. Guo, Q. Sun, N. Wang, R. Bai, J. Yu, *Chem. Commun.* **2018**, *54*, 3697-3700.
- [4] a) K. Hemelsoet, J. Van der Mynsbrugge, K. De Wispelaere, M. Waroquier, V. Van Speybroeck, *Chemphyschem* **2013**, *14*, 1526-1545; b) J. F. Haw, W. Song, D. M. Marcus, J. B. Nicholas, *Acc. Chem. Res.* **2003**, *36*, 317-326; c) W. Dai, G. Wu, L. Li, N. Guan, M. Hunger, *ACS Catal.* **2013**, *3*, 588-596; d) Z. Liu, X. Dong, Y. Zhu, A.-H. Emwas, D. Zhang, Q. Tian, Y. Han, *ACS Catal.* **2015**, *5*, 5837-5845.
- [5] a) Q. Sun, Y. Ma, N. Wang, X. Li, D. Xi, J. Xu, F. Deng, K. B. Yoon, P. Oleynikov, O. Terasaki, J. Yu, *J. Mater. Chem. A* **2014**, *2*, 17828-17839; b) Z. Li, J. Martínez-Triguero, J. Yu, A. Corma, *J. Catal.* **2015**, *329*, 379-388; c) S. Askari, R. Halladj, *Ultrason. Sonochem.* **2012**, *19*, 554-559; d) H. van Heyden, S. Mintova, T. Bein, *Chem. Mater.* **2008**, *20*, 2956-2963.
- [6] a) Y. Li, M. Zhang, D. Wang, F. Wei, Y. Wang, *J. Catal.* **2014**, *311*, 281-287; b) Y. Li, Y. Huang, J. Guo, M. Zhang, D. Wang, F. Wei, Y. Wang, *Catal. Today* **2014**, *233*, 2-7; c) S. H. Jhung, J.-S. Chang, J. S. Hwang, S.-E. Park, *Microporous Mesoporous Mater.* **2003**, *64*, 33-39.
- [7] a) M. Hartmann, A. G. Machoke, W. Schwieger, *Chem. Soc. Rev.* **2016**, *45*, 3313-3330; b) Q. Sun, N. Wang, D. Xi, M. Yang, J. Yu, *Chem. Commun.* **2014**, *50*, 6502-6505; c) X. Liu, S. Ren, G. Zeng, G. Liu, P. Wu, G. Wang, X. Chen, Z. Liu, Y. Sun, *RSC Adv.* **2016**, *6*, 28787-28791; d) C. Wang, M. Yang, W. Zhang, X. Su, S. Xu, P. Tian, Z. Liu, *RSC Adv.* **2016**, *6*, 47864-47872; e) F. Wang, L. Sun, C. Chen, Z. Chen, Z. Zhang, G. Wei, X. Jiang, *RSC Adv.* **2014**, *4*, 46093-46096; f) F. Schmidt, S. Paasch, E. Brunner, S. Kaskel, *Microporous Mesoporous Mater.* **2012**, *164*, 214-221; g) A. Z. Varzaneh, J. Towfighi, S. Sahebdelfar, *Microporous Mesoporous Mater.* **2016**, *236*, 1-12.
- [8] a) C. Wang, M. Yang, P. Tian, S. Xu, Y. Yang, D. Wang, Y. Yuan, Z. Liu, *J. Mater. Chem. A* **2015**, *3*, 5608-5616; b) P. Wu, M. Yang, W. Zhang, S. Xu, P. Guo, P. Tian, Z. Liu, *Chem. Commun.* **2017**, *53*, 4985-4988.
- [9] a) X. Chen, A. Vicente, Z. Qin, V. Ruau, J.-P. Gilson, V. Valtchev, *Chem. Commun.* **2016**, *52*, 3512-3515; b) Y. Qiao, M. Yang, B. Gao, L. Wang, P. Tian, S. Xu, Z. Liu, *Chem. Commun.* **2016**, *52*, 5718-5721; c) Z. Liu, S. Ren, X. Yu, X. Chen, G. Wang, X. Wu, G. Yu, M. Qiu, C. Yang, Y. Sun, *Catal. Sci. Technol.* **2018**, *8*, 423-427.
- [10] Q. Sun, N. Wang, R. Bai, X. Chen, J. Yu, *J. Mater. Chem. A* **2016**, *4*, 14978-14982.
- [11] D. Xi, Q. Sun, J. Xu, M. Cho, H. S. Cho, S. Asahina, Y. Li, F. Deng, O. Terasaki, J. Yu, *J. Mater. Chem. A* **2014**, *2*, 17994-18004.
- [12] W. Shen, X. Li, Y. Wei, P. Tian, F. Deng, X. Han, X. Bao, *Microporous Mesoporous Mater.* **2012**, *158*, 19-25.
- [13] a) W. Song, J. F. Haw, J. B. Nicholas, C. S. Heneghan, *J. Am. Chem. Soc.* **2000**, *122*, 10726-10727; b) E. Borodina, H. Sharbini Harun Kamaluddin, F. Meirer, M. Mokhtar, A. M. Asiri, S. A. Al-Thabaiti, S. N. Basahel, J. Ruiz-Martinez, B. M. Weckhuysen, *ACS Catal.* **2017**, *7*, 5268-5281.
- [14] a) Q. Qian, J. Ruiz-Martinez, M. Mokhtar, A. M. Asiri, S. A. Al-Thabaiti, S. N. Basahel, B. M. Weckhuysen, *ChemCatChem* **2014**, *6*, 772-783; b) D. Cai, Y. Ma, Y. Hou, Y. Cui, Z. Jia, C. Zhang, Y. Wang, F. Wei, *Catal. Sci. Technol.*, **2017**, *7*, 2440-2444.

Entry for the Table of Contents

FULL PAPER

A series of nano-sized SAPO-34 catalysts with tunable hierarchical structures are synthesized in the system of $\text{Al}_2\text{O}_3\text{-H}_3\text{PO}_4\text{-SiO}_2\text{-triethylamine(TEA)-H}_2\text{O}$ by using a mesoporegen-free nanoseed-assistant method. The nano-sized hierarchical $\text{S}_\text{H-3.0}$ catalyst ($\text{TEA}/\text{Al}_2\text{O}_3=3.0$) shows the highest selectivity of ethylene and propylene up to 85.4%, which reaches the top level in MTO reactions ever reported under the similar conditions.



Qiming Sun, Ning Wang, Risheng Bai, Guangrui Chen, Zhiqiang Shi, Yongcun Zou, and Jihong Yu*

Page No. – Page No.

Mesoporegen-Free Synthesis of Nano-sized Hierarchical SAPO-34 Zeolite with Reduced Template Consumption and Excellent MTO Performance